Light Metals 2012 *Edited by: Carlos E. Suarez*
TMS (The Minerals, Metals & Materials Society), 2012

Numerical Investigation of Bubble Dynamics in Aluminium Electrolytic Cells

Kaiyu Zhang[1, 2], Yuqing Feng[2], Phil Schwarz[2], Mark Cooksey[2], Zhaowen Wang[1]

1. Northeastern University, Shenyang Liaoning 110004, China
2. CSIRO, Box 312, Clayton South, VIC 3169, Australia

Keywords: computational fluid dynamics, aluminum reduction cell, bubble behavior

Abstract

Gas generated beneath anodes in aluminum electrolytic cells play an important role for the circulation of the bath, alumina mixing, and heat balance. Those bubbles cause an extra voltage drop, which is strongly affected by the amount and shape of the bubbles beneath anodes. Consequently, understanding the dynamic behavior of bubbles in aluminum electrolytic cells has been a major research focus worldwide in recent decades.

This paper presents a numerical investigation of the motion of a single bubble beneath an anode. Using a 2-dimensional geometry of part of a real cell, the motion of different sized bubbles has been simulated. It was found that the bubble size affects bubbling dynamics significantly as is measured by bubble shape, sliding velocity beneath anodes and bubble induced turbulence. Simulations have been also conducted using an air-water system to check its relevance to the CO_2-cryolite system.

Introduction

Gas generated beneath anodes in aluminum electrolytic cells is released in the form of bubbles. The bubbles play an important role for the circulation of the bath, alumina mixing, and heat balance. However, due to the poor electrical conductivity of gas, the bubbles beneath anodes introduce extra voltage drop, which is in the range of 0.15 to 0.35 V[1], a significant amount of extra energy loss. One study [2] showed that 100 mV fall in cell voltage corresponds to about 2% increase of current efficiency, which implies there is great potential for energy efficiency through a better control of the bubbling dynamics. The bubble motion beneath anodes also increases the instability of the bath-metal interface, producing greater voltage fluctuation. Therefore, a detailed understanding of the dynamic behavior of bubbles beneath anodes is necessary for better control of the process through optimized design and/or operation.

The hostile environment (high temperature and corrosive molten salt bath) restrict direct observation of bubble behavior in an industrial cell. Very limited data give information of the bubble detail behavior in real cell. Using a probe which transfers signal when it occasionally contacts with the gas bubble layer, Haupin [1] found the gas bubble layer under the margin of the anode bottom in a real cell is about 5mm, but the detailed bubble shape and bubble coverage is still not clear.

Laurent Cassayre [3] used a lab scale see-through crucible to investigate the bubble behavior. He found the gas prefers to nucleate at fixed points prior to a bubble growing, with the bubble thickness being around 4 mm which agrees well with other scientific work. However the tests were limited in time, anode-cathode distance (ACD) and scale of the crucible, because the crystalline walls of the see-through crucible quickly eroded in a couple of minutes, becoming opaque and restricting vision.

In order to observe the dynamic behavior of bubbles, many researchers applied transparent materials to construct the cell structure, and utilize room temperature liquid to replace the cryolite bath. Air-water room temperature models are often used with the gas being physically injected [4-6]. These studies are mainly focused on bubble induced liquid flow and it is commonly accepted that the air-water system can reasonably represent the real system as the water kinematic viscosity is very similar to that of the cryolite (8.93×10^{-7} m^2s^{-1} for water and 1.14×10^{-6} m^2s^{-1} for cryolite). Klara Vekony[7] stated that according to her previous mathematical simulation, the shape of a bubble depends, among other things, on the liquid's Morton number. A similar conclusion has been reported by other scientists [8]. As shown in Table 1, the Morton number for an air-water system is very different to that for the real cryolite system. Systems closer to the real electrolytic process were introduced using various electrolytes, such as NaOH solution [9], $CuSO_4$ solution[10], and air-oil-water[11, 12]. None of the studies can closely simulate the bubble formation and sliding motion beneath the anode as the bubble formation is much more complex and the motion is controlled by many factors, such as liquid viscosity, contact angle, surface tension, anode inclination angle, and even the roughness of the surface.

Computational fluid dynamics (CFD) modeling can account for these complexities and use the actual gas and liquid properties. Over the past two decades, with advances in computing speed, parallelization technology, improved software and multiphase algorithms, CFD has progressed substantially to a point where it can be used for prediction of complex gas-liquid flows such as those encountered in aluminium reduction cells. Depending on the application and information required, gas-liquid flow can be modeled at different length scales: at the individual bubble scale or at the macro level by local averaging. The former approach tracks the interfaces around each of the bubbles using for example the volume of fluid (VOF) method, and detailed transient bubbling behaviour can be obtained. The locally averaged model represents the flow field averaged over time and hence steady state equations are solved. The former model is suitable for fundamental studies, the latter for process simulation. Both models are widely used to study various gas-solid flow behaviour and are areas of major research at CSIRO[13, 14].

The individual bubble model provides an excellent opportunity to investigate the bubble dynamics beneath anodes and recently has been used to study an aluminium system with different focuses. Einarsrud[11] studied the effect of detaching bubbles on aluminium-cryolite interfaces; Das et al [15] investigated the principal characteristics of the detachment and sliding mechanism of gas bubbles under an inclined anode; Wang and Zhang[16]

studied the effect of the shape of the anode edge on bubble release. No literature gives a quantitative comparison of the difference between air-water and CO_2-cryolite systems.

This work aims to make a comparison between the two systems by numerical simulation of the detailed bubble motion beneath an anode using an individual bubble model. As an initial investigation, one bubble is simulated for each case using a 2-dimensional geometry of part of a real cell as the test-bed. The difference in bubble behavior due to the bubble sizes and the different properties between the air-water system and CO_2-cryolite real system are assessed in terms of bubble shapes, bubble thickness, sliding velocity, bubble coverage and drag coefficient. A Fortin type bubble is investigated in detail based on the surrounding hydrodynamics.

CFD Modelling Method

Model Description

Simulation of bubble moving phenomena requires accounting for the irregular deformation of the free surface. The free-surface flow can be modeled by interface-tracking method[17] and interface capturing method [18]. The interface-tracking method uses interface-fitted moving grids, while the interface-capturing methods uses fixed grids and solves an additional equation to locate the free surface. Considering the free surface can change its topology due to bubble breaking, overturning and splashing, the grid might be not able to deform to such an extent and even it did so, the computer cannot run such a big task. The interface-capturing method is popularly used.

There are many kinds of interface-capturing methods such as level set method[19], height of liquid[20] and volume of fluid (VOF)[21]. The classical VOF method is used in the current study since it is relatively effective in capturing the bubble dynamics. Ddetails of this method are well documented in literature[22].

Model Parameters

Though there is no technical difficulty in simulating the 3 dimensional (3D) motion of bubbles, because of limitations in simulation time and computing cost, the investigations are conducted using a 2 dimensional (2D) geometry. Figure 1 shows the 2D geometry used in the simulations. The geometry represents a slice of a typical commercial Hall–Héroult prebake cell, but is not related to any specific cell design. The ACD is 50 mm and the bath depth is 150 mm. An inclination of 1.5° (as might occur because of anode consumption) is set to help the release of bubbles. The initial geometry mesh (without refinement function) consists of 1624 quadrangle cells.

The formation of bubbles in an aluminium reduction cell is very complex and the detailed bubble formation mechanism is still not very clear. To model the bubble generation more realistically, a CFD model fully coupled with thermal and electric models is required. In this study, a simplified gas generation method is used. A bubble is set in a rectangular region beneath the anode close to the lowest end. The rectangular height is set 5 mm with the length varied to account for different bubble sizes. Given that the models of the two physical systems use the same bubble generation method, the simulation results are valid for comparison purposes.

Table 1 lists the physical properties of the two systems. Considering different sized bubbles co-exist in a real cell, the bubble is set with different sizes. For each system, three bubble sizes are used, 11.3, 22.6 and 33.9 mm in equivalent bubble diameter. Thus, as is listed in Table 2, a total of 6 cases are simulated.

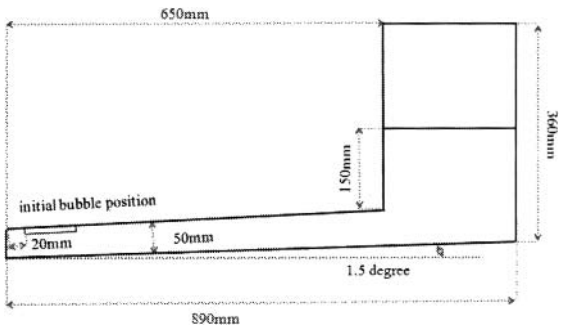

Figure 1: Geometry for a full-scale 2D cell half-anode cross sectional area of CFD model

Table 1: Physical properties of the CO_2-cryolite and the air-water systems

Properties	CO_2 at 960°C	Cryolite at 960°C	Air at 25°C	Water at 25°C
Density (kg/m^3)	0.4	2100	1.225	998.2
Dynamic viscosity ($kg/m \cdot s$)	1.37×10^{-5}	3.0×10^{-3}	1.789×10^{-5}	1.003×10^{-3}
Kinematic viscosity (m^2/s)	3.43×10^{-5}	1.43×10^{-6}	1.46×10^{-5}	1.005×10^{-6}
Surface tension (N/m)	0.132		0.072	
Contact angle (degree)	120°		60°	
Morton number	1.645×10^{-10}		2.664×10^{-11}	

Table 2: Simulation cases with different bubble sizes

	Equivalent bubble diameter (mm)	systems
Case 1	11.3	air-water
Case 2	11.3	CO_2-cryolite
Case 3	22.6	air-water
Case 4	22.6	CO_2-cryolite
Case 5	31.9	air-water
Case 6	31.9	CO_2-cryolite

Numerical Platform

In the present work, a commercial CFD package (ANSYS-Fluent) based on the Finite Element Method was used to achieve a numerical solution. A mesh adaption method[22] is used in this work, allowing more accurate capturing of the detailed interface between gas and liquid, and reducing computing time significantly. The mesh will be dynamically refined at the interface, and coarsened again when the interface moves out of that region. The maximum level of mesh refinement is set to be 8 in this work, and the minimal cell surface is set as 6.0×10^{-9} m^2. The global Courant number is set 0.3 to dynamically control the time step.

Results and Discussion

1. Bubble Morphology

The initial set of a rectangular shaped bubbles evolve to a smooth interface system in a period of about 0.5 seconds. The bubble reaches a dynamically stable state quickly and moves towards the higher end with various shapes that are dependent on bubble size and system. Figure 2 plots the bubble morphologies for all the simulation cases when their dynamically stable states are reached. For each case, the bubble shapes at three time frames are plotted.

For all the simulated bubble sizes, the bubble layer thickness is larger in air-water system than that in CO_2-cryolite system. The contact angle is the most likely reason for this difference. For both systems, the bubble tends to change its shape from a uniform flat shape to a non-regular shape with a thick head, and a long and thin tail as the bubble size increases.

The formation of different bubble shapes are actually a complex dynamic balance of surface tension, buoyancy force, viscosity friction between liquid and gas, solid wall friction and contact angle. When the bubble size is small, the specific surface area (ratio of surface area to the bubble volume) is large, which implies that unit volume gas receives larger surface tension for the smaller sized bubbles than for the larger size bubbles. Thus the bubble tends to form towards a more spherical form as bubble size decreases.

When the bubble size increases, the specific surface area decreases. The bubble tends to flatten out beneath the anodes. This way, the bubble receives less resistance when it slides along the anode. The higher velocity leads to more instability of the bubble surface. In the header, the gas motion will be suppressed by liquid in front, while gas at the back continuously moves forward. This will cause the head to expand in the vertical direction. Thus a thick head is formed. Such bubbles with thicker head and thinner tail are often called Fortin bubbles[23] after the first person to give a description of this type of bubble in a tilted anode surface. A detailed investigation of this Fortin type bubble is discussed in a later section.

Figure 3 shows the bubble mean thickness for all simulation cases. For both systems, the bubble thickness increases as the bubble size increases. At a given bubble size, the bubble thickness is larger in the air-water system than that in the CO_2-cryolite system. As the bubble size is fixed, a larger thickness implies less anode coverage. However, the larger bubble thickness leads to less bubble sliding velocity, thus the bubble residence time in ACD is larger.

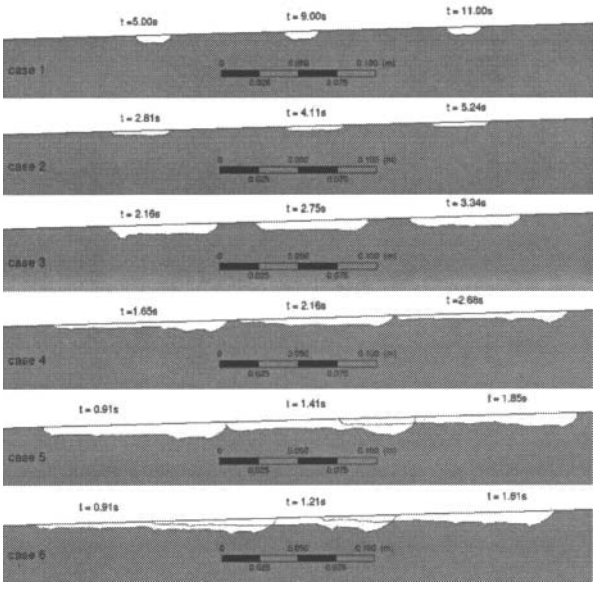

Figure 2: Bubble morphologies for different simulation cases at three different times when their dynamically stable state is reached.

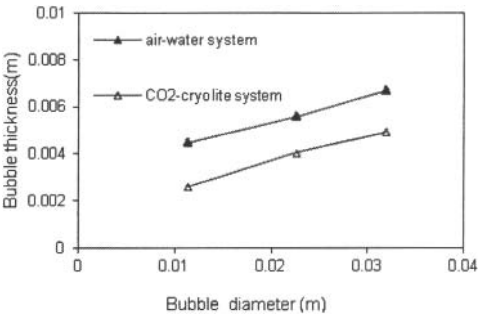

Figure 3: The mean bubble thickness as a function of bubble diameter for both systems

2. Bubble Sliding Velocity and Drag Coefficient

The motion of bubbles is further quantified by their mean velocity at their dynamically stable state. Figure 4 plots the mean bubble velocity at different bubble sizes for both investigated systems. The mean velocity increases as the bubble size increases for both systems. For a given bubble size, the bubble moves faster in the CO_2-cyolite system than that in the air-water system. This appears consistent with bubble shapes: as the bubble thickness is smaller in the CO_2-cryolite system, there is less resistance around the head.

The bubble induced voltage drop is closely related to bubble coverage area and gas layer thickness. The bubble coverage area will have much larger effect than bubble thickness [24]. As shown in Figure 3, the bubble coverage area is larger in the CO_2-cryolite

system than that in the air-water system. However, the bubble moves faster beneath the anode. A combined consideration of individual bubble length and bubble velocity is needed to compare the bubble coverage for the two systems. This will be investigated in the future.

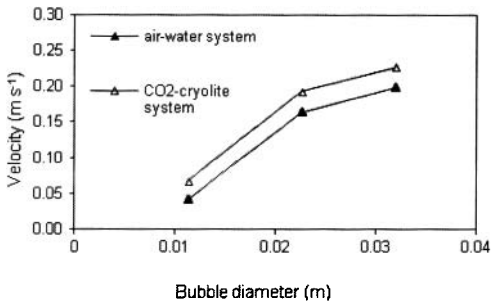

Figure 4: Variation of the mean bubble velocity for different bubble sizes and systems when their dynamically stable state is reached.

Figure 5 plots the drag coefficient at different bubble sizes for the two systems. The drag coefficient reduces as the bubble size increases. There is a very large difference when the bubble size is small. The difference reduces as the bubble size increases. For a given bubble size, the air-water system leads to a larger drag coefficient. The drag force value is quite small in comparison to that in free vertical bubbling flow. According to Ishii Zuber's correlation, the drag coefficient is about 2.4 in this bubbling region. A proper set of drag coefficents is required in the local averaged model for process scale simulation, where the drag coefficient determines the interface momentum exchange. In the previous study of full cell model using the local averaged model, the drag coefficient in ACD is simply set as the same as the vertical flow or arbitrarily set with a small value[13, 25-30]. Consequently, the present quantification of the drag coefficient foe bubbles in the in ACD provides execellent information for improving modelling accuracy of process scale simulations.

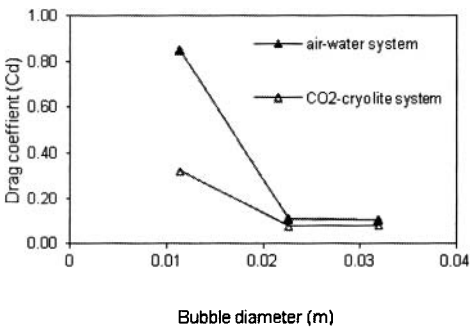

Figure 5: The drag coefficient of bubbles as a function of bubble diameter within different bath environments

3. The Formation of Fortin Type Bubbles

This study uses three bubble sizes. In a real system, the flow must be very complex. The large bubbles move faster than the small bubbles. The bubbles will coalescence to form bigger bubble when the large bubbles catch up with the small bubbles. The bubble will break up when the bubble size grows too large. For a tilted anode system, the Fortin bubbles might be dominant though different sized bubbles co-exist. Therefore, the final analysis is focused on the bubbling dynamics of Fortin type bubbles.

The cause of Fortin type bubbles has been investigated using experiment by Vekony and Kiss [7]. A Fortin type bubble has been observed either with the bubble head towards the higher end of the anode or with the bubble head towards the lower end of the anode, depending on liquid flow direction.

Figure 6 re-plots a schematic diagram from Fortin et al [23]'s work, which gives a qualitative information on the formation of Fortin bubble. In comparison with their work, Figure 7 plots some detailed hydrodynamic information around a Fortin bubble obtained from CFD simulation. Interestingly, the shape and streamlines from CFD simulation (Figure 7 A, B, C) are very similar to the past experiment (Figure 6).

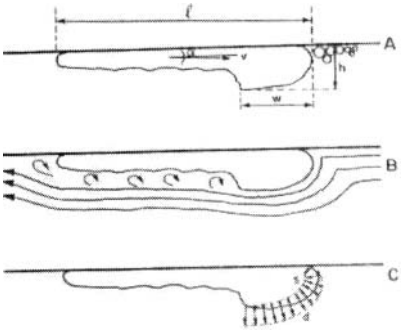

Figure 6: Schematic of hydrodynamics around a Fortin bubble [23]: (A) Typical profile of a large bubble travelling up the anode slope; (B) Streamlines generated by the relative motion of the bubble and electrolyte. Boundary layer separation occurs at the downstream end of the bubble head resulting in a turbulent region down-stream; (C) Hydrostatic, s, and hydro-dynamic, d, pressure distributions along the bubble front.

The gravity induced buoyancy component i.e. parallel to the underneath of the anode is the main cause of the bubble drifting along the anode while the perpendicular component flattens the shape of the bubble.

It is apparent from Figure 7(D) that no obvious pressure gradient is found within the bubble and the total pressure in the flat bubble is almost uniform and the value is always equal to the pressure in the liquid at the three-phase contact line. The value of static pressure of the liquid around the bubble is due to the liquid level and liquid density.

Features within the bubble are strongly influenced by the resistance of the liquid environment as the bubble moves. This influence is greater around the interface of the bubble: as the bubble moves ahead, the bubble gas molecules around the head surface change the original dynamic state and move backward along the bubble profile due to the viscosity stress drag by the liquid and this induces a relative motion within the bubble, as shown in Fig 7(E).

Obviously, the velocity adjacent to the head surface is lower than the velocity in the core position of the bubble head as shown in Figure 7(F), where these two regions of different relative velocities meet, a clear typical vortex forms around the cusp part (shown in red line) of the head.

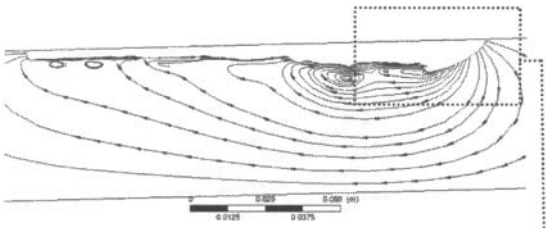

(A) Streamlines around the typical Fortin type bubble

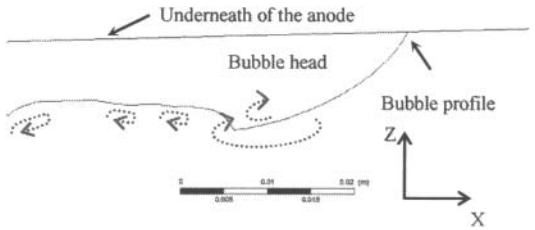

(B) Typical profile of Fortin bubble head travelling under the anode

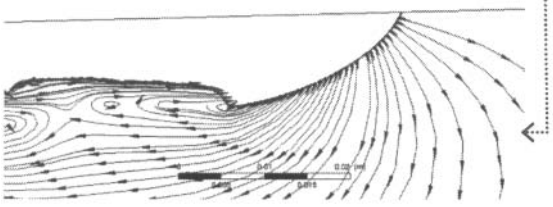

(C) Streamlines around the typical Fortin bubble head

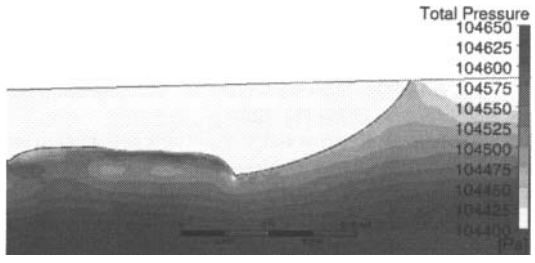

(D) Total pressure contour distribution

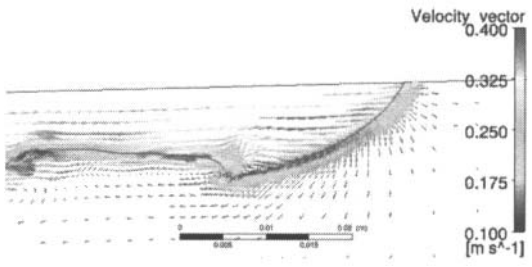

(E) Velocity vector distribution

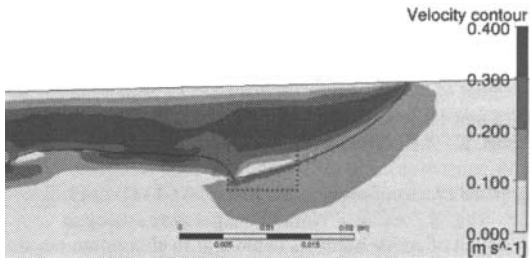

(F) Velocity contour distribution

Figure 7: Flow dynamics around a Fortin type bubble for case 6 at time 1.00 s: (A) Streamlines around the typical Fortin type bubble; (B) Typical profile of a large bubble head travelling right up the anode slope. The red lines represent the vortexes around the head; (C) Streamlines around the typical Fortin bubble head; (D) Total pressure (Hydrostatic and hydrodynamic pressure) distribution along the bubble front; (E) Velocity vector around the bubble. Boundary layer separation occurs at the trailing edge of the bubble head resulting in the turbulent region downstream due to the vortex; (F) Velocity contour features around the Fortin bubble head which imply relative motion within the bubble and around the bubble interface

Conclusions

By applying an advanced VOF-CFD model with mesh adaption technology, and using a 2D simulation domain of part of an aluminium cell, the bubbling dynamics beneath anodes have been investigated for both air-water and CO2-cryolite systems. The results demonstrate that both systems show a similar trend of dynamics as bubble size increases, i.e. a regular shape at small bubble sizes and the formation of Fortin type bubble when the bubble size increases, with increase in sliding velocity as the bubble size increases.

Quantitatively, there are some differences between the two systems. For a fixed size, the CO2-cryolite system leads to a larger bubble sliding velocity and a smaller bubble thickness than in the air-water system.

The formation of Fortin type bubbles is investigated based on detailed hydrodynamics around the bubble. Following the motion of the bubble towards the higher end of the anode, the bubble squeezes liquid in front causing it to move downward and backward. The opposite movement between the gas and liquid leads to a strong shear at the interface, which forms a local vortex. A strong vortex is formed around $1/3^{rd}$ to $1/4^{th}$ of the distance from the bubble head, and this point separates the bubble into a thick head and thin tail.

Acknowledgments

The work is financially supported by CSIRO Mineral Down Under Flagship.

Kaiyu Zhang thanks for the China Scholarship Council (CSC) for a visiting PhD scholarship.

References

1. Haupin, W., "A scanning reference electrode for voltage contours in alumium smelting cells." *Journal of Metals*, 23(10)(1971), 46-49.
2. Shiying, S., "Why energy consumption of aluminium electrolysis stops decreasing in recent years."(Paper presented at conference on Up to date Aluminium Smelter Technology, Zhenzhou China, 2000)
3. Cassayre, L., et al., "Gas evolution on graphite and oxygen-evolving anodes during aluminium electrolysis", *Light Metals*, 2 (2006), 379-383
4. E. Dernedde, "Gas induced circulation in aluminium reduction cell", *Light Metals* (1975),111-122
5. Nikitin.A.V and Kryukovskll.V.A., "Gas impregnation and speed of anode gas flow in high-powered aluminum reduction cells." *Tsvetnye Metally/Non-Ferrous Metal*, 16(8)(1975), 37-40.
6. Cooksey, M.A. and W. Yang, "PIV measurements on physical models of aluminium reduction cells." *Light Metals* 2(2006), 359-365.
7. Vekony, K. and L.I. Kiss, "Morphology of Two-Phase Layers with Large Bubbles." *Metallurgical and Materials Transactions B-Process Metallurgy and Materials Processing Science*, 41(5)(2010), 1006-1017.
8. Perron, A., L.I. Kiss, and S. Poncsak, "Regimes of the movement of bubbles under the anode in an aluminum electrolysis cell." *Light Metals*,(2005), 565-570.
9. Qian, K., Z.D. Chen, and J.J.J. Chen, "Bubble coverage and bubble resistance using cells with horizontal electrode." *Journal of Applied Electrochemistry*, 28(10)(1998), 1141-1145.
10. Y. Xue, N.Z.a.C.B., "Normal temperature analogue experiment of anode bubble's behaviour in aluminium electrolysis cells." *The Chinese Journal of Nonferrous Metals*, 2006,1823-1828.
11. Einarsrud, K.E., "The Effect of Detaching Bubbles on Aluminum-Cryolite Interfaces: An Experimental and Numerical Investigation." Metallurgical and Materials Transactions B-*Process Metallurgy and Materials Processing Science*, 41(3)(2010), 560-573.
12. D.C. Chesonis, A.F.L.C., "Influence of gas-driven circulation on alumina distribution and interface motion in a Hall-Héroult cell." *Light Metals*, 1990, 211-220.
13. Y. Feng, W.Yang., M. Cooksey and P. Schwarz, "Development of bubble driven flow CFD model applied for aluminium smelting cells." *The Journal of Computational Multiphase Flows*, (2010), 179-188.
14. Lane, G.L., M.P. Schwarz, and G.M. Evans, "Numerical modelling of gas-liquid flow in stirred tanks." *Chemical Engineering Science*. 60(8-9)(2005), 2203-2214.
15. S. Das, Y.M., G. Brooks, W. Yang and J.J.J. Chen, "The principal characteristics of the detachment and sliding mechanism of gas bubble under an inclined anode." *10th Australasian Aluminium Smelting Technology Conference*,(2011).
16. Zhang. Y.F,Wang.L.F., "Numerical modelling on the fluid flow-related phenomena in an aluminium electrolysis cell." *Light Metals*, (2010), 14-18.
17. Heo, N. and H.-S. Ko, "Detail-Preserving Fully-Eulerian Interface Tracking Framework". *Acm Transactions on Graphics*, 29(6)(2010),176..
18. Tezduyar, T.E., "Interface-tracking and interface-capturing techniques for finite element computation of moving boundaries and interfaces." *Computer Methods in Applied Mechanics and Engineering*, 195(23-24)(2006), 2983-3000.
19. Malladi, R., J.A. Sethian, and B.C. Vemuri, "Shape M\odeling with Front Propagation - A Level Set Approach." *Ieee Transactions on Pattern Analysis and Machine Intelligence*, 17(2)(1995), 158-175.
20. Morales, R.E.M. and E.S. Rosa, "Modeling of free surface flow in a helical channel with finite pitch." *Journal of the Brazilian Society of Mechanical Sciences and Engineering*, 29(4)(2007), 345-353.
21. Severo, D.S., et al., "Modeling magnetohydrodynamics of aluminum electrolysis cells with ANSYS and CFX." *Light Metals* (2005), 475-480.
22. ANSYS Fluent User Manual (2010), ANSYS INC.
23. Fortin, S., M. Gerhardt, and A.J. Gesing, "Physical Modeling of Bubble Behavior and Gas-Release From Aluminum Reduciton Cell Anodes." *Journal of Metals*, 35(12)(1984), 95-95.
24. Cooksey, M.A., M.P. Taylor, and J.J.J. Chen, "Resistance due to gas bubbles in aluminum reduction cells". *JOM*, 60(2)(2008), 51-57.
25. Y.Q. Feng, M. Cooksey and P. Schwarz, "CFD modeling for improvement of alumina feeding system in Aluminum reduction cells", TMS Annual Meeting, 27, Feb – 3 Mar, 2011, San Diego, USA.
26. Y.Q. Feng, M. Cooksey and P. Schwarz, "CFD modelling of alumina mixing in aluminium reduction cells", TMS Annual Meeting, 14-18, Feb, 2010. Seattle, USA, pp.100-106.
27. Y.Q. Feng, W. Yang, M. Cooksey and P. Schwarz, "Development of bubble driven flow CFD model applied for aluminium smelting cells", Seventh International Conference on Computational Fluid Dynamics in the Process Industries, 9-11 December 2009, Melbourne, Australia. (CD Rom)
28. Y.Q. Feng, M. Cooksey and P. Schwarz, "Development of whole cell CFD model of bath flow and aluminium mixing", 9th Australasian Aluminium Smelting Technology Conference and Workshop, Terrigal, NSW, 4-9 November 2007, (CD Rom).
29. Y.Q. Feng, M. Cooksey and P. Schwarz, "CFD modeling of gas liquid flow in Aluminum smelting", *Light Metals,* 2007, pp. 339-334.
30. Y.Q. Feng, W. Yang, M. Cooksey and P. Schwarz, "CFD model of bubble driven flow in aluminium reduction cells and validation using PIV measurement", Fifth International Conference on Computational Fluid Dynamics in the Process Industries, 13-15 December 2006, Melbourne, Australia (CD Rom Edition)